

## ON THE EXISTENCE OF PULSARS IN THE VICINITY OF THE MASSIVE BLACK HOLE IN THE GALACTIC CENTER

FUPENG ZHANG<sup>1,2</sup>, YOUJUN LU<sup>1</sup> & QINGJUAN YU<sup>2</sup>

<sup>1</sup> National Astronomical Observatories, Chinese Academy of Sciences, Beijing, 100012, China; luyj@nao.cas.cn

<sup>2</sup> Kavli Institute for Astronomy and Astrophysics, Peking University, Beijing, 100871, China; zhangfupeng, yuqj@pku.edu.cn

*Draft version March 12, 2018*

### ABSTRACT

Pulsars, if existing and detectable in the immediate vicinity of the massive black hole (MBH) in the Galactic center (GC), may be used as a superb tool to probe both the environment and the metric of the central MBH. The recent discovery of a magnetized pulsar in the GC suggests that many more pulsars should exist near the MBH. In this paper, we estimate the number and the orbital distribution of pulsars in the vicinity of the MBH in the GC by assuming that the pulsar progenitors, similar to the GC S-stars, were captured to orbits tightly bound to the MBH through the tidal breakup of stellar binaries. We use the current observations on both the GC S-stars and the hypervelocity stars to calibrate the injection rate(s) of and the dynamical model(s) for the stellar binaries. By including the relaxation processes, supernova kicks, and gravitational wave radiation in our simulations, we estimate that  $\sim 97 - 190$  ( $9 - 14$ ) pulsars may presently orbit the central MBH with semimajor axes  $\leq 4000$  AU ( $\leq 1000$  AU), which is compatible with the current observational constraints on the number of the GC pulsars. The semimajor axis and the pericenter distance of the pulsar closest to the central MBH are probably in the range of  $\sim 120 - 460$  AU and  $\sim 2 - 230$  AU, respectively. Future telescopes, such as the SKA, may be able to detect a significant number of pulsars with semimajor axis smaller than a few thousand AU in the GC. Long-term monitoring of these pulsars would be helpful in constraining both the environment and the metric of the central MBH. Our preferred model also results in about ten hyperfast pulsars with velocity  $\gtrsim 1500\text{km s}^{-1}$  moving away from the Milky Way.

*Subject headings:* Black hole-physic-Galaxy: center - Galaxy: kinematics and dynamics - (stars:) pulsars: general

### 1. INTRODUCTION

Long term monitoring of the motion of the S-stars<sup>1</sup> located at the Galactic center (GC) demonstrates exclusively the existence of a massive black hole (MBH) in the GC (e.g., Ghez et al. 2008; Gillessen et al. 2009). Although the source confusion in observations has so far inhibited the discovery of any star rotating around the MBH with an orbital period  $< 10$  yr (Meyer et al. 2012), young stars and compact stars, including neutron stars and stellar mass black holes, are expected to exist in this region (e.g., Miralda-Escudé & Gould 2000; Angéilil et al. 2010; Liu et al. 2012; Zhang et al. 2013). If some of these stars are radio pulsars, which would be promising in observational detection and providing a superb clean tool to probe the gravitational field of the central MBH (e.g., Paczynski & Trimble 1979; Pfahl & Loeb 2004; Angéilil et al. 2010). It becomes especially encouraging that a magnetar, a highly magnetized pulsar, is recently discovered at a parsec (pc) distance from the central MBH. This magnetar has been used to reveal the magnetic field in the GC (see Rea et al. 2013; Eatough et al. 2013; Kennea et al. 2013; Mori et al. 2013). Magnetars are a rare type of pulsars, and the discovery of a magnetar in the GC suggests that many more normal pulsars exist there.

The GC S-stars may be the captured components of stellar binaries that were tidally broken up in the vicinity of the central MBH as proposed by Gould & Quillen

(2003, see also Ginsburg & Loeb 2006; Löckmann et al. 2008; Perets 2009; Antonini & Merritt 2013; Zhang et al. 2013). The other components of those broken-up binaries may be ejected to the Galactic halo as hypervelocity stars (HVSs; e.g., Hills 1988; Yu & Tremaine 2003; Brown et al. 2005; Edelmann et al. 2005; Hirsch et al. 2005; Brown et al. 2012). Zhang et al. (2013, hereafter ZLY13; see also Lu et al. 2010, and Zhang et al. 2010) find that the current observations on both the GC S-stars and the HVSs are compatible with the model that their progenitorial stellar binaries are originated from the young stellar disk(s) at a distance of  $0.04 - 0.5$  pc from the MBH (Lu et al. 2009; Bartko et al. 2009).

Assuming that both the HVSs and the GC S-stars are produced by the tidal breakup mechanism, the injection rate of stellar binaries to the immediate vicinity of the central MBH can be constrained by using current observations on the numbers and distributions of these two populations. Some of the captured/ejected massive components (with mass  $\geq 9M_{\odot}$ ; Heger et al. 2003) of the broken-up binaries may collapse and explode to form pulsars at the end of their main-sequence lives. Therefore, the number of the pulsars currently existing in the GC can be reasonably estimated if adopting the tidal breakup mechanism to produce the massive GC S-stars. Pfahl & Loeb (2004) estimated the number of the pulsars existing in the vicinity of the central MBH ( $\lesssim 4000$  AU)<sup>2</sup> to be  $\sim 1000$  (see also a new

<sup>1</sup> Hereafter denoted as the GC S-stars.

<sup>2</sup> Different units for the distance of a star from the GC MBH are chosen in different references, e.g., pc in Liu et al.

estimate on the pulsar generation rate in the GC by Dexter & O’Leary 2013). In this paper, we revisit the estimation by including more detailed and realistic considerations of various physical processes involved in, such as the dynamical evolution of the pulsars and their progenitors, the kicks received by the pulsars at their birth, and the orbital decay due to the gravitational wave (GW) radiation, etc.

This paper is organized as follows. In Section 2, we perform a large number of full three-body experiments to realize the tidal breakup processes of stellar binaries in the vicinity of the central MBH by adopting different binary injection models. We follow the dynamical evolution of the captured components, by considering the resonant and the non-resonant relaxations due to background stars, and the decay due to the GW radiation. If a captured (or an ejected) star ends its main-sequence life and explodes to form a pulsar before the end of the simulation, the motion of the pulsar is assumed to receive a kick at its birth, based on a kick-velocity distribution obtained from observations. We set the end of the simulations as the present time. We follow the kinematic motions of the ejected components in the Galactic potential and obtain the number and the spatial distribution of HVSs at the present time. The parameters describing the initial settings for each hypothesized injection model can be calibrated by using current observations as done in ZLY13. With the calibrated model parameters, the number and the spatial distribution of these pulsars are estimated in Section 3. We further estimate the probability distributions of the semimajor axis and the pericenter distance of the inner most pulsar. Discussion and conclusions are given in Section 4.

## 2. MONTE-CARLO SIMULATIONS

### 2.1. Model Settings

We first perform a large number of Monte-Carlo three-body experiments to realize the tidal breakup processes of stellar binaries in the vicinity of the central MBH and generate the mock samples of the GC S-stars and the HVSs. We adopt the code DORPI5 based on the explicit fifth(fourth)-order Runge-Kutta method to simulate the three-body interaction between a stellar binary and the MBH (Dormand & Prince 1980; Haier et al. 1993). For details of the simulation, see Zhang et al. (2010). Similar to ZLY13, we also adopt several injection models with different settings on the origin of the stellar binaries and the distributions of their properties, denoted as “Unbd-MS0”, “Disk-TH0”, “Disk-TH2”, “Disk-IM0”, and “Disk-IM2”, respectively (see Table 1, and also Section 3.1 in ZLY13).

- The progenitorial stellar binaries are assumed to be originated either from disk structure(s) like the clockwise rotating stellar disk in the GC (the last four models) or from infinity with initial velocities

(2012) and Gillessen et al. (2009), mas ( $10^{-3}$  arcsec) in Ghez et al. (2008), and gravitational radius  $r_g$  in Angéil et al. (2010), respectively. For the GC MBH system, we note here that  $1\text{mas} \simeq 3.88 \times 10^{-5} \text{pc}(R_{GC}/8\text{kpc}) \simeq 8\text{AU}(R_{GC}/8\text{kpc}) \simeq 202r_g(M_\bullet/4 \times 10^6 M_\odot)^{-1}(R_{GC}/8\text{kpc})$ . In this paper, the MBH mass is set to be  $M_\bullet = 4 \times 10^6 M_\odot$ , the distance from the GC to the sun is  $R_{GC} = 8\text{kpc}$ , and we mainly use the physical distance unit AU to describe the distance of a GC star from the central MBH.

of  $250\text{kms}^{-1}$  (the first model), which are represented by the “Disk” and “Unbd” in the model notations, respectively.

- Current observations show that the initial mass function (IMF) of the young stars in the GC is  $-1.7$  (see Lu et al. 2013) or  $-0.45$  (see Bartko et al. 2010). The IMF estimated by Lu et al. (2013) is consistent with the constraint obtained from the number ratio of the HVSs to the GC S-stars if both of them are produced by the tidal breakup of stellar binaries originated from the stellar disk(s) in the GC (see ZLY13). We adopt the Miller-Scalo IMF ( $\gamma = -2.7$ ) for the Unbd-MS0 model, an IMF with a slope of  $\gamma = -1.6$  (denoted as an intermediate slope) for the Disk-IM0 model and the Disk-IM2 model, and a top-heavy IMF with  $\gamma = -0.45$  for the Disk-TH0 model and the Disk-TH2 model, which are denoted as the “MS”, “IM” and “TH” in the model notations, respectively. The number “0” and “2” in the model notations represent that the distribution of the initial pericenter distances  $r_{p,i}$  of the injecting binaries approaching the MBH follows a power law, i.e.,  $\propto r_{p,i}^\beta$ , with a slope  $\beta = 0$  or  $\beta = 2$ , respectively. The total number of three-body experiments is  $10^5$  for each model. For details of the initial settings and other properties of the stellar binaries in these injection models, see ZLY13.

We assume that the stellar binaries injected (or migrated) into the vicinity of the central MBH and were tidally broken-up soon after their formation, therefore, all stars were on the main-sequence before they were captured by the MBH or ejected from the GC. We assume a constant injection rate of stellar binaries over the past 250Myr in each model, which can be calibrated by the observational statistical properties of the GC S-stars (and/or the HVSs) as done in ZLY13. We follow the dynamical evolution of the captured components by adopting the Auto-Regressive Moving Average (ARMA) model given by Madigan et al. (2011), in which both the resonant and the non-resonant relaxations are considered (see also Section 4 in ZLY13 for details). The background stars are the main objects that cause both the resonant and the non-resonant relaxations of the captured GC S-stars and pulsars. Recent observations suggest that the density of those background stars can be modeled by a core density profile (e.g., Do et al. 2009). Therefore, we adopt a power-law density distribution for the background stars, i.e.,  $\rho_* \propto r^{-\alpha}$ , with  $\alpha = 0.5$ , to mimic the effect of a core-like distribution (see also Madigan et al. 2011 and ZLY13). We will also discuss the effect on the results by choosing a Bahcall-Wolf cusp  $\alpha = 7/4$  (Bahcall & Wolf 1976) in Section 3.

In our calculations, we remove those captured stars that approach the MBH within the tidal radius, i.e.,  $(2M_\bullet/m_*)^{1/3}R_*$ , where  $m_*$  and  $R_*$  are the stellar mass and radius, because they should be tidally disrupted and swallowed by the central MBH. We also follow the kinetic motions and evolution of the ejected components in the Galactic potential (for details see Section 5 in ZLY13).

### 2.2. GC pulsars and Supernova Kick

TABLE 1

Model	$\gamma$	$\beta$	core-like profile ( $\alpha = 0.5$ )			Bahcall-Wolf cusp ( $\alpha = 7/4$ )		
			$N_{\text{P}}^{\text{obs}}$	$N_{\text{ej}}^{\text{obs}}$	$N_{\text{kick}}^{\text{obs}}$	$N_{\text{P}}^{\text{obs}}$	$N_{\text{ej}}^{\text{obs}}$	$N_{\text{kick}}^{\text{obs}}$
Unbd-MS0	-2.70	0	38 (52)	33 (47)	0 (0)	31 (43)	45 (59)	0 (0)
Disk-TH0	-0.45	0	96 (391)	54 (199)	1 (2)	76 (336)	62 (241)	1 (2)
Disk-TH2	-0.45	2	128 (470)	8 (31)	2 (7)	100 (406)	8 (36)	3 (6)
Disk-IM0	-1.60	0	61 (126)	33 (61)	1 (1)	48 (100)	36 (69)	0 (0)
Disk-IM2	-1.60	2	97 (190)	4 (8)	2 (3)	69 (152)	5 (9)	3 (4)

NOTE. — Numbers of the ejected and the captured pulsars at the present time obtained from different models. The injection rate of stellar binaries is assumed to be a constant over the past 250 Myr, which is calibrated by producing 17 GC S-stars with semimajor axis  $< 4000$  AU for each model.  $N_{\text{P}}^{\text{obs}}$ ,  $N_{\text{ej}}^{\text{obs}}$  and  $N_{\text{kick}}^{\text{obs}}$  represent the number of pulsars with semimajor axis  $\leq 4000$  AU at the end of the simulation, the total number of pulsars with velocity  $\geq 1500 \text{ km s}^{-1}$  at infinity, and the number of those pulsars with velocity  $\geq 1500 \text{ km s}^{-1}$  at infinity that are originally simulated GC S-stars but were kicked out from the GC due to supernova explosions, respectively. The numbers listed in the fourth column to sixth column and the seventh column to ninth column are obtained by adopting a core-like density profile and a Bahcall-Wolf cusp for the background stars, respectively. From the fourth to ninth columns, the numbers within (or out of) brackets represent the results obtained by assuming that those simulated GC S-stars with mass  $\geq 9M_{\odot}$  (or in the range of  $9M_{\odot} - 25M_{\odot}$ ) can turn to pulsars when they end their main-sequence life.

The captured massive stars may evolve into pulsars/neutron stars after their main-sequence lives. According to Heger et al. (2003) and Georgy et al. (2009), stars with mass in the range of  $9 - 25M_{\odot}$  can turn into pulsars/neutron stars, while some with mass above  $25M_{\odot}$  stars may turn into pulsars/neutron stars only if their metallicities are above the solar abundance. Observational constraints on the progenitor mass of pulsars are more or less consistent with theoretical expectations (e.g., Smartt 2009). It has been shown that the metallicities of the GC S-stars may be higher than the solar abundance (e.g., Paumard et al. 2006). Therefore, we consider two extreme cases in this study: (a) only those simulated GC S-stars and HVSSs with mass in the range  $9 - 25M_{\odot}$  can evolve into pulsars once they end their main-sequence lives; and (b) all those simulated GC S-stars and HVSSs with mass  $\geq 9M_{\odot}$  can turn into pulsars once they end their main-sequence lives. We assume the active time of these pulsars is  $\sim 100$  Myr. In this study, we mainly focus on case (a) if not otherwise stated; the numbers of pulsars resulting from case (a) are taken as the reference numbers, and those from case (b) may be taken as the upper limits.

A pulsar formed through the collapse of a massive star may receive a kick at its birth. According to pulsar observations, the one-dimensional component of this kick velocity follows an exponential distribution as estimated by Faucher-Giguère & Kaspi (2006), i.e.,

$$P(v_l) = \frac{1}{2 \langle |v_l| \rangle} \exp\left(-\frac{|v_l|}{\langle |v_l| \rangle}\right), \quad (1)$$

where  $v_l$  is the one-dimensional component of the 3D velocity,  $\langle |v_l| \rangle = 180_{-30}^{+20} \text{ km s}^{-1}$ .<sup>3</sup> According to Equation (1), we randomly assign each component of a 3D kick velocity  $\delta\vec{v}$  to each newly born pulsar, and consequently the directions of the 3D kick velocities for pulsars are randomly distributed. By receiving such a kick, the

<sup>3</sup> Adopting a different kick velocity distribution [i.e., as that estimated by Arzoumanian et al. (2002), or Cordes & Chernoff (1998), or Lyne & Lorimer (1994), or Hansen & Phinney (1997)], the resulting numbers of active pulsars may increase or decrease by only  $\lesssim 20\%$ .

specific energy  $E$  and angular momentum  $\vec{J}$  of a pulsar change by

$$\delta E_{\text{kick}} = \vec{v}_{\text{orb}} \cdot \delta\vec{v} + \frac{1}{2} |\delta\vec{v}|^2, \quad (2)$$

and

$$\delta \vec{J}_{\text{kick}} = \vec{r}_{\text{orb}} \times \delta\vec{v}, \quad (3)$$

respectively, where  $\vec{r}_{\text{orb}}$  and  $\vec{v}_{\text{orb}}$  are the position vector and the orbital velocity of the pulsar, respectively. The changes of the specific energy and angular momenta due to the supernova kick are included in the ARMA model according to Equations (2) and (3) above.

### 2.3. Orbital Decay due to the Gravitational Wave Radiation

For those pulsars with extremely high orbital eccentricities  $e$  and small semimajor axes  $a$ , the GW radiation may be important for their orbital evolution. The GW decay timescale for an object, with mass  $m$ , eccentricity  $e$ , and semimajor axis  $a$ , is given by (Peters 1964)

$$T_{\text{GW}} \sim 1.2 \times 10^8 \text{ yr} \frac{f(0.99)}{f(e)} \left(\frac{1.4M_{\odot}}{m}\right) \times \left(\frac{a}{300 \text{ AU}}\right)^4 \left(\frac{M_{\bullet}}{4 \times 10^6 M_{\odot}}\right)^{-3}, \quad (4)$$

and

$$f(e) \equiv (1 - e^2)^{-7/2} \left(1 + \frac{73}{24}e^2 + \frac{37}{96}e^4\right). \quad (5)$$

The GW decay timescale  $T_{\text{GW}}$  can be comparable to the active time of pulsars if  $m \sim 1.4M_{\odot}$ ,  $a \sim 300$  AU and  $e \sim 0.99$ . We modify the ARMA model by adding additional terms in the evolution of their orbital energy  $E$  and momenta  $J$  in order to include this GW effect on the orbital evolution of the GC pulsars (and also the GC S-stars) (see Peters 1964), i.e.,

$$\delta E = P \frac{dE}{dt} = -\frac{32 G^4 m M_{\bullet}^3}{5 c^5 a^5} \frac{1 + \frac{73}{24}e^2 + \frac{37}{96}e^4}{(1 - e^2)^{7/2}} \times P, \quad (6)$$

$$\delta J = P \frac{dJ}{dt} = -\frac{32 G^{7/2} m M_{\bullet}^{5/2}}{5 c^5 a^{7/2}} \frac{1 + \frac{7}{8}e^2}{(1 - e^2)^2} \times P, \quad (7)$$

where  $G$  is the gravitational constant,  $c$  is the light speed, and  $P = 2\pi(a^3/GM_\bullet)^{1/2}$  is the orbital period of a pulsar (or a GC S-star).

For the secular evolution of the orbits of pulsars/stars, we consider the periastron advances due to the general relativity correction and the orbital decay due to the gravitational radiation in the ARMA model. We neglect the effects due to other low-order post-Newtonian terms (such as the Lense-Thirring precession and the frame dragging, etc.) for the following reasons. (1) The magnitude of the Lense-Thirring precession is relatively much smaller than that of the periastron advance, and the periastron advance has been included in the ARMA model (see ZLY13 and Madigan et al. 2011); (2) the other low-order post-Newtonian effects do not lead to secular orbital decay of those pulsars; and (3) although those effects may affect the orbital motion of individual stars in the vicinity of the MBH (e.g., see Iorio 2011; Angélic et al. 2010), we obtain the evolution of the GC system in a *statistical* way through the ARMA model, which should be sufficient for the purpose of the study presented here.

We trace the motions of those newly born pulsars until the end of our simulations. For each pulsar, the calculation is terminated if its age reaches 100 Myr (which is assumed to be the lifetime of active pulsars) or if it is swallowed by the central MBH. If the lifetime of active pulsars is shorter than the assumed one, the number of the resulting pulsars decreases proportionally. A pulsar can directly plunge into and be swallowed by the central MBH if its angular momentum is less than  $4GM_\bullet/c$  (and thus on an unstable orbit; e.g., Chandrasekhar 1983, Ivanov 2002), although the tidal radius of the pulsar is smaller than the MBH event horizon. We remove those pulsars with angular momenta  $\leq 4GM_\bullet/c$  from our calculations.

### 3. RESULTS

We record the simulated GC S-stars, HVSSs and active pulsars at the end of the Monte-Carlo simulations for each model. Figure 1 shows the cumulative distributions of the semimajor axis and eccentricity for both the simulated GC S-stars (thin lines) and the pulsars (thick lines) obtained from different models. As seen from Figure 1, the resulting distributions of the semimajor axis and eccentricity of the simulated GC S-stars are more or less statistically compatible with the observations (see also discussions in ZLY13). Further in consideration of the ratio of the number of the HVSSs to that of the GC S-stars and the velocity distribution of HVSSs, the Disk-IM2 model may match the observations better (see also detailed analysis in ZLY13). The distributions of the semimajor axis and the eccentricity of the active pulsars appear to be quite different from those of the GC S-stars, which is mainly due to: (1) the supernova kicks received by pulsars at their birth, and (2) the dynamical evolution timescale of the active pulsars ( $10^8$  yr) is substantially longer than those of the GC S-stars (at most a few times  $10^7$  yr).

For each model, we count the total number of those simulated GC S-stars with mass in the range of  $\sim 7 - 15M_\odot$  and semimajor axes  $a \leq 4000$  AU, denoted as  $N_S^{\text{sim}}$ ; and we also count the final number of those simulated active pulsars with  $a \leq 4000$  AU, denoted as  $N_P^{\text{sim}}$ .

As the total number of the detected GC S-stars with  $a \leq 4000$  AU is known to be  $N_S^{\text{obs}} = 17$  (Gillessen et al. 2009), therefore, the total number of active pulsars at the present time can be estimated as  $N_P^{\text{obs}} = N_S^{\text{obs}} N_P^{\text{sim}} / N_S^{\text{sim}}$  for each model. By doing so, we estimate the total number of active pulsars (with  $a \leq 4000$  AU) at the present time for each model as listed in Table 1. The Disk-IM2 model may match the statistical properties of both the GC S-stars and the HVSSs better as demonstrated in ZLY13, therefore, the total number of active pulsars with semimajor axes  $\leq 4000$  AU (or  $\leq 1000$  AU) is  $\sim 97 - 190$  (or  $\sim 9 - 14$ ) in the preferred DISK-IM2 model if choosing a core-like density profile for the background stars. If choosing a Bahcall-Wolf cusp for the background stars, this number decreases slightly to  $\sim 69 - 152$  (or  $\sim 4 - 7$ ). The decrease of the number of the resulting pulsars is due to that the resonant relaxation process is more efficient in the case of a Bahcall-Wolf cusp than that of a core-like density profile, which leads to more pulsars being excited to extremely high eccentric orbits and being swallowed by the central MBH (see also discussions in ZLY13). The estimated number is smaller than the previous estimation ( $\sim 1000$  by Pfahl & Loeb 2004) by one order of magnitude. The main reason for this difference is that we further consider the dynamical model of capturing stars by the central MBH in details, the effect of the IMF, the dynamical evolution of the GC S-stars and pulsars, and the effect of the kick received by a newly formed pulsar at its birth, etc. For example, more than 25% of the pulsars are ejected out from the immediate vicinity of the central MBH to infinity because of the kicks received by these pulsars at their birth.

#### 3.1. The Innermost Pulsar

The pulsar with the smallest semimajor axis (and pericenter distance), if detectable, should be most helpful in probing the strong gravitational field and constraining the metric of the central MBH. In order to check whether it is possible to find a pulsar that is sufficiently close to the central MBH, we estimate the probability distributions of the semimajor axis and the eccentricity of the innermost pulsar resulting from each model above. To do so, we first randomly select  $N_P^{\text{obs}}$  pulsars from those active pulsars resulting from each model and record the properties of the one with the smallest semimajor axis among them. We repeat this procedure by  $10^6$  times, and then use the recorded innermost pulsars to obtain the probability distributions of the semimajor axis and the pericenter distance for the innermost active pulsar.

Figure 2 shows the probability density distributions of the semimajor axis (left panel) and the pericenter distance (right panel) of the innermost pulsar resulting from different models, where  $P(x)$  is defined so that  $P(x)dx$  is the probability of being in the range of  $x \rightarrow x + dx$ . As seen from Figure 2, the Disk-TH0 model results in an innermost pulsar relatively closer to the central MBH than all the other models. The semimajor axis distributions obtained from the Unbd-MS0 model and the Disk-IM0 model (or from the Disk-TH2 model and the Disk-IM2 model) are similar; and the models with small  $\beta$  ( $= 0$ ) result in an innermost pulsar more closer to the central MBH than the models with large  $\beta$  ( $= 2$ ; see the left panel of Figure 2), as more binaries were injected into the immediate vicinity of the central MBH in the models

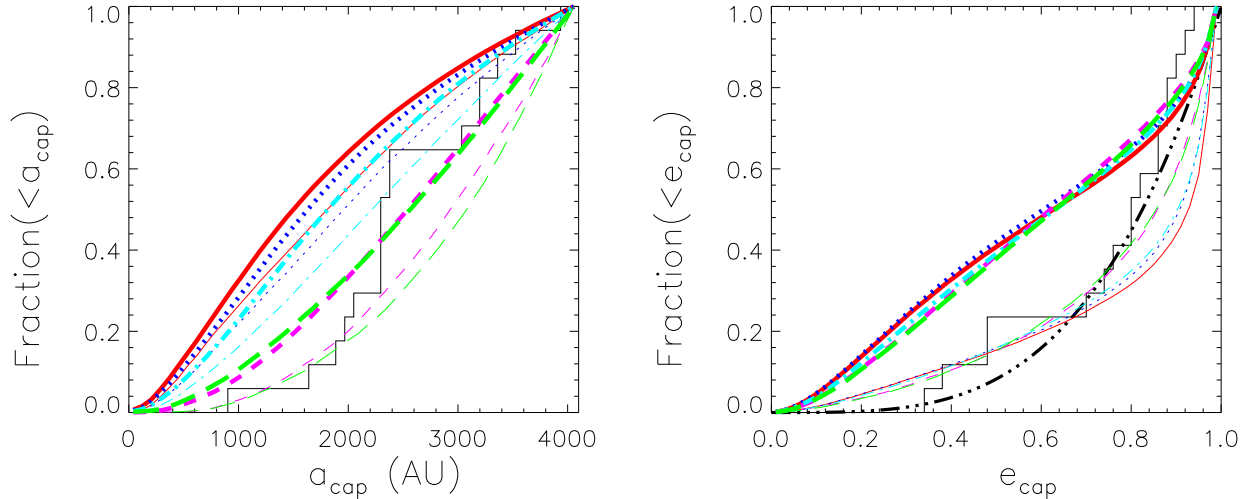


FIG. 1.— Cumulative distributions of the semimajor axis (left panel) and the eccentricity (right panel) of the captured stars (thin lines) and pulsars (thick lines) with semimajor axis  $\leq 4000$  AU surviving to the present time, respectively. The solid (red), dotted (blue), dashed (magenta), dot-dashed (cyan) and long-dashed (green) curves represent the results obtained from the Unbd-MS model, the Disk-TH0 model, the Disk-TH2 model, the Disk-IM0 model, and the Disk-IM2 model, respectively. In each panel, the histogram represents the distribution of the observed GC S-stars (Gillessen et al. 2009). In the right panel, the black dot-dot-dot-dashed line represents a cumulative distribution proportional to  $e_{\text{cap}}^{3.6}$  as suggested by the observations (Ghez et al. 2008; Gillessen et al. 2009).

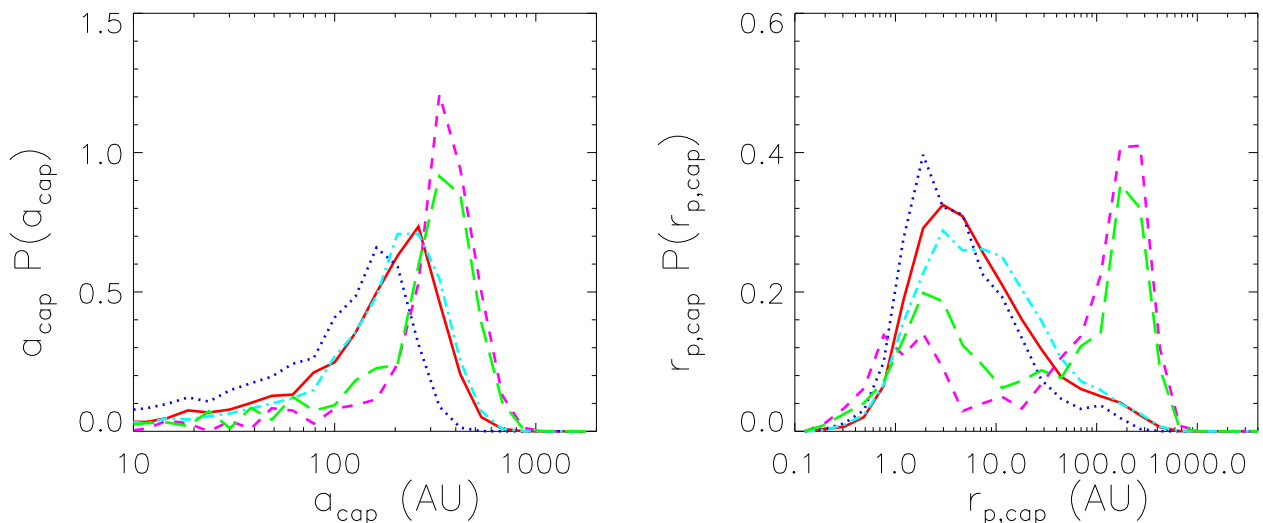


FIG. 2.— Probability density distributions of the semimajor axis (left panel) and the pericenter distance (right panel) of the innermost pulsar at the present time. The solid (red), dotted (blue), dashed (magenta), dot-dashed (cyan) and long dashed (green) curves represent the results obtained from the Unbd-MS model, the Disk-TH0 model, the Disk-TH2 model, the Disk-IM0 model, and the Disk-IM2 model, respectively. The estimates shown here are obtained by (1) assuming that the captured stars with mass in the range of  $9 - 25M_{\odot}$  all turn into pulsars after their main-sequence lives; and (2) calibrating the injection rate of stellar binaries over the past 250 Myr to generate 17 GC S-stars at the present time, the same number as that of the observed ones.

with  $\beta = 0$  than that in the models with  $\beta = 2$ .

Note there are two peaks in the pericenter distance distribution of the innermost pulsar resulting from the Disk-TH2 model and the Disk-IM2 model (see the short dashed and long dashed lines in the right panel of Figure 2). The left peak (close to the MBH) is due to that the orbits of a number of pulsars, with small semimajor axes and large eccentricities (e.g.,  $a_{\text{cap}} \sim 300$  AU and  $e \gtrsim 0.99$ ), decay rapidly due to the GW radiation, while the right peak (further away from the MBH) represents those pulsars that are not significantly affected by the GW radiation.

As a comparison to the dynamical evolution of the GC pulsars, the GW radiation plays little role in the orbital

evolution of the simulated GC S-stars. The reasons for this are two folds: first, the lifetime of the simulated GC S-stars is only  $\sim 10^7$  yr, which is much less than the GW decay timescale as these stars typically have semimajor axes larger than a few hundred AU; second, for those simulated GC S-stars that can be excited to extremely highly-eccentric orbits ( $e > 0.99$ ), their orbits decay fast due to the GW radiation but they are more likely to be tidally disrupted and swallowed by the central MBH rather than survive to the present time.

We define the most probable range of the semimajor axis (or the pericenter distance) of the innermost pulsar here as the range from 16 percentile to 84 percentile of the distributions, which is  $57 - 303$  AU ( $2 - 24$  AU),

31 – 211 AU (1 – 14 AU), 199 – 461 AU (2 – 256 AU), 76 – 322 AU (2 – 30 AU), and 116 – 461 AU (2 – 228 AU), for the Unbd-MS0 model, the Disk-TH0 model, the Disk-TH2 model, the Disk-IM0 model, and the Disk-IM2 model, respectively. For all the models, including the reference model (Disk-IM2), the semimajor axis of the resulting innermost pulsar is  $\lesssim 300 - 500$  AU (corresponding to a period of  $\sim 2.6 - 5.6$  yr), substantially smaller than that of the currently known GC S-stars. According to the probability distributions shown in Figure 2, the probability of the innermost pulsar with semimajor axis  $\leq 300$  AU (or  $\leq 100$  AU) is 83% (26%), 98% (43%), 33% (8%), 79% (22%), and 45% (15%), for the Unbd-MS0 model, the Disk-TH0 model, the Disk-TH2 model, the Disk-IM0 model, and the Disk-IM2 model, respectively. The existence of such a pulsar, if detectable, should provide a superb tool to probe the metric and determine the spin of the central MBH. As pointed out by Liu et al. (2012, see also Angéilil et al. 2010; Pfahl & Loeb 2004) that the frame-dragging signal or even higher order general relativistic effects could be detected by using the pulsar timing of a pulsar orbiting the central MBH with a semimajor axis smaller than a few hundred AU if the timing accuracy is moderately high (e.g.,  $\lesssim 10^{-4}$  s).

In fact, not every pulsar can be detected because of many factors, including the beaming effect and the scattering of radio wave by turbulent ionized gas between the pulsar and the observer. Assuming that optimistically 10% of the normal pulsars can be detected by future facilities, such as the Square Kilometer Array (SKA) (see Equation 2 in Pfahl & Loeb 2004), we also estimate the probability distributions of the semimajor axis and the eccentricity of the innermost “*detected*” pulsar for each model, which are shown in Figure 3. The most probable range of the semimajor axis (pericenter distance) of the innermost “*detected*” pulsar is 340 – 1424 AU (7 – 791 AU), 211 – 754 AU (4 – 286 AU), 468 – 1350 AU (27 – 791 AU), 306 – 1151 AU (8 – 631 AU), and 468 – 1423 AU (21 – 791 AU) for the Unbd-MS0 model, the Disk-TH0 model, the Disk-TH2 model, the Disk-IM0 model, and the Disk-IM2 model, respectively. For majority of the models, the semimajor axis of the resulting innermost pulsar is probably still smaller than that of the currently known GC S-stars. However, the probability of the “*detected*” innermost pulsar with semimajor axis  $\leq 300$  AU (or  $\leq 100$  AU) is only 13% (2%), 31% (4%), 4% (0.6%), 15% (2%), and 5% (1%) for the Unbd-MS0 model, the Disk-TH0 model, the Disk-TH2 model, the Disk-IM0 model, and the Disk-IM2 model, respectively. As the probability is not negligible, there might be still some chance to find a pulsar sufficiently close to the central MBH by future facilities that may help to constrain the MBH metric.

For case (b), i.e., all captured stars with mass  $> 9M_{\odot}$  turn to active pulsars when they end their main-sequence life, then the probability that the innermost “*detected*” pulsar has a semimajor axis  $\leq 300$  AU is 85% (or 16%), 100% (64%), 78% (14%), 97% (27%), and 52% (7%) for the Unbd-MS0 model, the Disk-TH0 model, the Disk-TH2 model, the Disk-IM0 model, and the Disk-IM2 model, respectively, if all (or only 10% of) the resulting pulsars can be detected. These probabilities are larger than that obtained for case (a) above, which may

strengthen the above conclusion that a pulsar substantially close to the central MBH may be found by future facilities and help to constrain the MBH metric.

If alternatively adopting a Bahcall-Wolf cusp for the background stars for case (a), the probability of the innermost “*detected*” pulsar with semimajor axis  $\leq 300$  AU is 42% (or 5%), 74% (12%), 18% (2%), 43% (5%), and 34% (3%) for the Unbd-MS0 model, the Disk-TH0 model, the Disk-TH2 model, the Disk-IM0 model, and the Disk-IM2 model, respectively, if all (or only 10% of) the resulting pulsars can be detected. These resulting probabilities are only slightly different from that obtained above by adopting a core-like density profile for the background stars. Therefore, qualitatively our main results are not affected by choosing a Bahcall-Wolf cusp for the background stars.

The pulsars generated above are all formed by the collapse and explosion of the captured components of stellar binaries that were tidally broken up in the vicinity of the central MBH. It is possible that other mechanism(s) may also bring pulsars to the immediate vicinity of the central MBH. For example: (1) some binaries with a pulsar component (or even two pulsar components) may be injected into the vicinity of the MBH and then tidally broken up with the pulsar component being captured. However, most of newly formed pulsars should be kicked out from binary systems by receiving the kicks due to supernovae explosion, and stay in isolate far away from the central MBH. It is reasonable to simply ignore the contribution by this mechanism. (2) Some isolated pulsars formed in the outer region of the GC (e.g., Zubovas et al. 2013; Baruteau et al. 2011) may migrate into the immediate vicinity of the central MBH via two-body relaxation. The typical timescales of the two-body relaxation in the S-star cluster region ( $\sim 10^9$  yr or larger; see Hopman & Alexander 2006; Yu et al. 2007) are far larger than the active time of pulsars ( $\sim 10^8$ yr). Therefore, the active pulsars within 4000 AU from the MBH should not be dominated by the pulsars resulting from the above two ways. In summary, our results on the number and orbital distribution of the pulsars with semimajor axis  $\leq 4000$  AU are not significantly affected by considering the above two mechanisms.

### 3.2. Hyperfast Pulsars

Some hyperfast pulsars can also be produced by the process of tidal breakup of stellar binaries in the vicinity of the central MBH (see Gavaramadze et al. 2008). There are two routes to form such hyperfast pulsars in the scenario of tidal breakup of stellar binaries.

- Collapse and explosion of massive HVSSs. In our simulations, many HVSSs, with mass  $\geq 9M_{\odot}$ , ended their main-sequence lives and collapsed to form pulsars before the end of the calculations. The ejection velocities of those HVSSs are already high (e.g.,  $\gtrsim 1000\text{km s}^{-1}$ ). The pulsars formed from those HVSSs can be further accelerated to even high velocities (e.g.,  $\gtrsim 1500\text{km s}^{-1}$ ) by the kicks received at its birth if the directions of these kicks are close to the velocity vectors of the progenitorial HVSSs.
- Collapse and explosion of some massive captured stars in the vicinity of the central MBH. The pul-

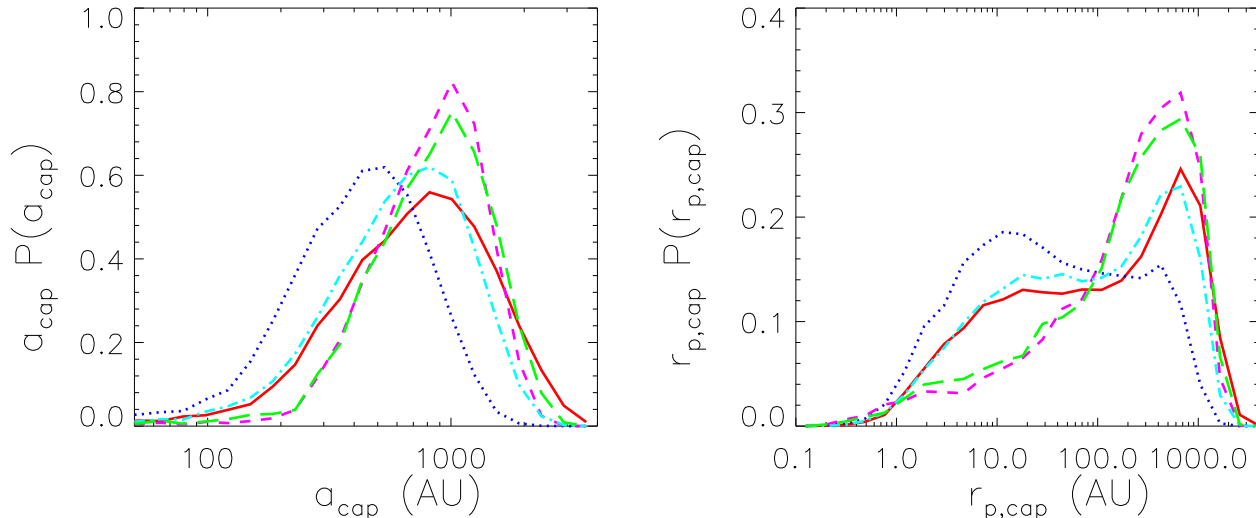


FIG. 3.— Legend similar to Figure 2, except that it is for the innermost “detected” pulsar by assuming that only 10% of the simulated pulsars can be detected.

sars formed via this route also receive kicks at its birth and may thus gain energy and be ejected out from the GC with hyperfast velocities. According to the energy conservation law, the ejection velocity of pulsar is  $v_{\text{ej}} \sim (2\delta v \sqrt{GM_{\bullet}/r_{\text{exp}}} - M_{\bullet}G/a_{\text{cap}})^{1/2}$ , where  $\delta v = |\delta \vec{v}|$  is the kick velocity,  $r_{\text{exp}}$  is the distance to the central MBH where the star explodes to form a pulsar, and  $a_{\text{cap}}$  is the semimajor axis of the progenitorial captured star. If  $a_{\text{cap}} \gg r_{\text{exp}}$ , we have

$$v_{\text{ej}} \sim 1500 \text{ km s}^{-1} \left( \frac{250 \text{ AU}}{r_{\text{exp}}} \right)^{1/4} \times \left( \frac{M_{\bullet}}{4 \times 10^6 M_{\odot}} \right)^{1/4} \left( \frac{\delta v}{300 \text{ km s}^{-1}} \right)^{1/2}. \quad (8)$$

For most simulated GC S-stars ( $a_{\text{cap}} \sim 1000 - 4000 \text{ AU}$ ), they can turn into hyperfast pulsars and be ejected out to the Galactic halo/bulge only if they explode at a location close to their periapsis.

Table 1 lists the number of the hyperfast pulsars (with velocities  $\geq 1500 \text{ km s}^{-1}$ ) via the first route and the second route, respectively. The reference model (Disk-IM2) only produces several to about 10 hyperfast pulsars that populate in the Galactic halo, while the Disk-TH0 model can produce  $\sim 50 - 200$  hyperfast pulsars. Only a small fraction of these hyperfast pulsars may be beaming toward us, so that the detectable ones among them are not many. As seen from Table 1, the majority of the hyperfast pulsars are produced by the collapse and explosion of massive HVSs; and the contribution from the collapse and explosion of the captured massive stars is insignificant as only a small fraction of the massive captured stars exploded near their periapses can lead to the ejection of hyperfast pulsars.

The hyperfast pulsars formed through the above two routes have velocities substantially larger than that formed in isolation or binaries. According to equation (1), the fraction of pulsars that can be kicked out to hyper-velocities  $> 1500 \text{ km s}^{-1}$  is about  $\sim 10^{-3}$ . The current number of known pulsars is  $\sim 2000$ . There-

fore, there could be a few hyperfast pulsars having velocities  $> 1500 \text{ km s}^{-1}$  formed in isolation or in binaries, and these hyperfast pulsars could be mixed with those formed through the above two routes. Future pulsar surveys may find some hyperfast pulsars. However, it is not easy to identify whether a hyperfast pulsar is originated from the GC or not as the motion of a hyperfast pulsar formed through the first route could deviate significantly from the radial motion because of the supernova kick.

#### 4. CONCLUSIONS AND DISCUSSIONS

In this paper, we estimate the number and orbital distribution of the pulsars currently existing in the vicinity of the MBH in the GC, by assuming that these pulsars are formed from the captured components of the massive binaries tidally broken up in the vicinity of the MBH. We follow the orbital evolution of those pulsars (and its progenitorial stars) by considering the effects of the limited stellar lifetime, the supernova kicks, the resonant and the non-resonant relaxations due to background stars, and the GW radiation. For the model that can simultaneously re-produce the statistical properties of both the observed GC S-stars and HVSs (i.e., the Disk-IM2 model), the number of pulsars with semimajor axis  $\leq 4000 \text{ AU}$  (or  $\leq 1000 \text{ AU}$ ) is estimated to be about 97 – 190 (or 9 – 14). Among them, the closest one to the central MBH probably has a semimajor axis and pericenter distance in the range of 116 – 461 AU and 2 – 228 AU, respectively.

The existence of pulsars in the GC is suggested by a number of indicative observations, including the pulsar wind nebular discovered by Wang et al. (2006), many X-ray binaries discovered by Munro et al. (2005) and Bower et al. (2005) at a distance within one parsec from the MBH, and a magnetar recently discovered within a parsec distance from the central MBH (see Rea et al. 2013; Kennea et al. 2013; Mori et al. 2013; Eatough et al. 2013), etc. The discovery of the magnetar is most encouraging because magnetars, i.e., the magnetized pulsars, are a rare type of pulsars; the discovery of a single magnetar in the central pc region is almost exclusively indicating the existence of a substantial number of normal pulsars within that region.

Recent systematic searches for pulsars did not detect

any but gave an upper limit of  $\sim 90$  normal pulsars in orbits within the central pc of Sgr A\* (e.g., Macquart et al. 2010; Eatough et al. 2012). The non-detection of pulsars in the GC for those searches may be partly due to that pulsar signals are strongly smeared by the hyper-strong scattering of radio waves by the turbulent ionized gas within the central 100 pc of Sgr A\*. The pulse broadening has a strong frequency dependence,  $\propto \nu^{-4}$ , making it nearly impossible to detect any pulsar in the GC at the typical observing frequencies of  $< 1.4$  GHz. It may be possible to avoid of this smearing problem by searching pulsars at high frequencies ( $> 10$  GHz). Chennamangalam & Lorimer (2013) revisited the constraint on the number of potential observable pulsars according to the current observations by adopting more realistic assumptions; they found a conservative upper limit  $\sim 950$  for the pulsars in orbits within the central pc.

The non-detection of pulsars in the GC is still compatible with our estimate of the number of the pulsars there ( $\sim 97 - 190$ , see Table 1). According to the method to estimate the number of observable pulsars developed in Codres & Lazio (1997), the fraction of observable pulsars in the GC by the current facilities is  $\sim 10^{-2}$  (see Equation 2 in Pfahl & Loeb 2004). As the expected total number of pulsars in the GC, with semimajor axes  $\leq 4000$  AU, is only  $\sim 97 - 190$ , the detectable pulsars would be only  $\sim 1 - 2$  (or even zero) by the current facilities.

Future radio telescopes, such as the SKA, may be able to detect 10% of the pulsars (see Equation 2 in Pfahl & Loeb 2004). We expect that ten to twenty (about one) pulsars will be discovered with semimajor axis  $\leq 4000$  AU ( $\leq 1000$  AU) in the GC by the SKA. Among the “detected” pulsars, the closest one to the central MBH probably has semimajor axis and pericenter distance in the range of 468 – 1423 AU and 21 – 791 AU,

respectively. For other models that can produce 17 GC S-stars as observed, the total number of the “detected” pulsars, with semimajor axes  $\leq 4000$  AU ( $\leq 1000$  AU), are about 4 – 50 (1 – 10), and the one closest to the central MBH may have a semimajor axis smaller than that resulting from the Disk-IM2 model. Long term monitoring of those pulsars close to the central MBH would be helpful in constraining the environment and the metric of the central MBH.

Our preferred model also results in about ten hyperfast pulsars with velocities  $\geq 1500$  km s $^{-1}$  moving away from the Milky Way, and most of them are produced by supernovae explosions of the massive HVs ejected from the GC. Some of these hyperfast pulsars may be detected by the SKA in the future. However, it is not easy to confirm that these hyperfast pulsars are originated from the GC solely by their moving directions.

QY thanks Scott Tremaine for communications on supernova kick. YL and QY acknowledge the hospitality of the KITP at Santa Barbara, where part of this work was written. This work was supported in part by the National Natural Science Foundation of China under nos. 11273004 and 11373031, the National Science Foundation under Grant No. NSF PHY11-25915, the Strategic Priority Research Program “The Emergence of Cosmological Structures” of the Chinese Academy of Sciences, Grant No. XDB09000000, and a grant from the John Templeton Foundation and National Astronomical Observatories of Chinese Academy of Sciences. The opinions expressed in this publication are those of the author(s) do not necessarily reflect the views of the John Templeton Foundation or National Astronomical Observatories of Chinese Academy of Sciences. The funds from John Templeton Foundation were awarded in a grant to The University of Chicago which also managed the program in conjunction with National Astronomical Observatories, Chinese Academy of Sciences.

#### REFERENCES

- Angéilil, R. and Saha, P. and Merritt, D., 2010, *ApJ*, 720, 1303  
 Antonini, F., & Merritt, D. 2013, *ApJ*, 763, L10  
 Arzoumanian, Z., Chernoff, D. F., & Cordes, J. M. 2002, *ApJ*, 568, 289  
 Bahcall, J. N., & Wolf, R. A. 1976, *ApJ*, 209, 214  
 Bartko, H., Martins, F., Fritz, T. K., et al. 2009, *ApJ*, 697, 1741  
 Bartko, H., Martins, F., Trippe, S., et al. 2010, *ApJ*, 708, 834  
 Baruteau, C., Cuadra, J., & Lin, D. N. C. 2011, *ApJ*, 726, 28  
 Bower, G. C., Roberts, D. A., Yusef-Zadeh, F., Backer, D. C., Cotton, W. D., Goss, W. M., Lang, C. C., & Lithwick, Y. 2005, *ApJ*, 633, 218  
 Brown, W. R., Geller, M. J., Kenyon, S. J., & Kurtz, M. J. 2005, *ApJL*, 622, L33  
 Brown, W. R., Geller, M. J., & Kenyon, S. J. 2012, *ApJ*, 751, 55  
 Chandrasekhar, S. 1983, *The Mathematical Theory of Black Holes*, Oxford University Press, Oxford  
 Chennamangalam, J., & Lorimer, D. R. 2013, arXiv:1311.4846  
 Dexter, J., & O’Leary, R. M. 2013, arXiv:1310.7022  
 Do, T., Ghez, A. M., Morris, M. R., Lu, J. R., Matthews, K., Yelda, S., & Larkin, J. 2009, *ApJ*, 703, 1323  
 Dormand, J. R., & Prince, P. J. 1980, *J. Comp. Appl. Math.*, Vol.6, p.19  
 Cordes, J.M., & Lazio, T.J. W. 1997, *ApJ*, 475, 557  
 Cordes, J. M., & Chernoff, D. F. 1998, *ApJ*, 505, 315  
 Eatough, R. P., Kramer, M., Klein, B., et al. 2012, arXiv:1210.3770  
 Eatough, R. P., Falcke, H., Karuppusamy, R., et al. 2013, *Nature*, 501, 391  
 Edelmann, H., Napiwotzki, R., Heber, U., Christlieb, N. & Reimers, D. 2005, *ApJL*, 634, L181  
 Faucher-Giguère, C.-A. & Kaspi, V. M. 2006, *ApJ*, 643, 332  
 Gvaramadze, V. V., Gualandris, A., & Portegies Zwart, S. 2008, *MNRAS*, 385, 929  
 Georgy, C., Meynet, G., Walder, R., Folini, D., & Maeder, A. 2009, *A&A*, 502, 611  
 Ghez, A., Salim, S., Weinberg, N. N., et al. 2008, *ApJ*, 689, 1044  
 Gillessen, S., Eisenhauer, F., Trippe, S., Alexander, T., Genzel, R., Martins, F., & Ott, T. 2009, *ApJ*, 692, 1075  
 Ginsburg, I., & Loeb, A. 2006, *MNRAS*, 368, 221  
 Gould, A., & Quillen, A. 2003, *ApJ*, 592, 935  
 Hairer, E., Norsett, S. P., & Wanner, G. Solving ordinary differential equations I. Nonstiff problems, Springer Series in Comput. Mathematics, Vol. 8, Springer-Verlag 1987  
 Hansen, B. M. S., & Phinney, E. S. 1997, *MNRAS*, 291, 569  
 Heger, A., Fryer, C. L., Woosley, S. E., Langer, N., & Hartmann, D. H. 2003, *ApJ*, 591, 288  
 Hills, J. 1998, *Natur*, 331, 687  
 Hirsch, H. A., Heber, U., O’Toole, S. J. & Bresolin, F. 2005, *A&A*, 444, L61  
 Hopman, C., & Alexander, T. 2006, *ApJ*, 645, 1152  
 Iorio, L. 2011, *Ph. Rev. D.*, 84, 124001  
 Ivanov, P. B. 2002, *MNRAS*, 336, 373

- Kennea, J. A., Burrows, D. N., Kouveliotou, C., et al. 2013, *ApJ*, 770, L24
- Liu, K., Wex, N., Kramer, M., Cordes, J. M., & Lazio, T. J. W. 2012, *ApJ*, 747, 1
- Löckmann, U., Baumgardt, H., & Kroupa, P. 2008, *ApJL*, 683, L151
- Lu, J. R., Ghez, A. M., Hornstein, S. D., Morris, M. R., Becklin, E. E., & Matthews, K. 2009, *ApJ*, 690, 1463
- Lu, J. R., Do, T., Ghez, A. M., Morris, M. R., Yelda, S., & Matthews, K. 2013, *ApJ*, 764, 155
- Lu, Y., Zhang, F., & Yu, Q. 2010, *ApJ*, 709, 1356
- Lyne, A. G., & Lorimer, D. R. 1994, *Natur*, 369, 127
- Macquart, J.-P., Kanekar, N., Frail, D. A., & Ransom, S. M. 2010, *ApJ*, 715, 939
- Madigan, A. M., Hopman, C., & Levin, Y., 2011, *ApJ*, 738, 99
- Meyer, L., Ghez, A. M., Schödel, R., et al. 2012, *Sci*, 338, 84
- Miralda-Escudé, J., & Gould, A. 2000, *ApJ*, 545, 847
- Mori, K., Gotthelf, E. V., Zhang, S., et al. 2013, *ApJ*, 720, L23
- Muno, M. P., Pfahl, E., Baganoff, F. K., Brandt, W. N., Ghez, A., Lu, J., & Morris, M. R. 2005, *ApJL*, 622, L113
- Pfahl, E., & Loeb, A. 2004, *ApJ*, 615, 253
- Paczynski, B., & Trimble, V. 1979, in Burton W. B., ed., *Proc. IAU Symp. 84, The Large-Scale Characteristics of the Galaxy*. Reidel, Dordrecht, p. 401
- Paumard, T., Genzel, R., Martins, F., et al. 2006, *ApJ*, 643, 1011
- Perets, H. B. Gualandris, A., Kupi, G., Merritt, D., & Alexander, T. 2009, *ApJ*, 702, 884
- Peters, P. C. 1964, *Phy. Rev.*, 136, 1224
- Rea, N., Esposito, P., Pons, J. A., et al. 2013, *ApJL*, 775, 34
- Smartt, S. J. 2009, *ARA&A*, 47, 63
- Wang, Q. D., Lu, F. J., & Gotthelf, E. V. 2006, *MNRAS*, 367, 937
- Yu, Q., Lu, Y., & Lin, D. N. C. 2007, *ApJ*, 666, 919
- Yu, Q., & Tremaine, S. 2003, *ApJ*, 599, 1129
- Zhang, F., Lu, Y., & Yu, Q. 2010, *ApJ*, 722, 1744
- Zhang, F., Lu, Y., & Yu, Q. 2013, *ApJ*, 768, 153
- Zubovas, K., Wynn, G. A., & Gualandris, A. 2013, *ApJ*, 771, 118